physica **pss** status solidi **b**

www.pss-b.com

basic solid state physics

Structural and electronic properties of wurtzite $B_xAl_{1−x}N$ from first-principles calculations

Muwei Zhang and Xiaohang Li*

King Abdullah University of Science and Technology (KAUST), Advanced Semiconductor Laboratory, Thuwal 23955-6900, Saudi Arabia

* Corresponding author: e-mail xiaohang.li@kaust.edu.sa, Phone: +966 012 808 7335

The structural and electronic properties of wurtzite $B_xAl_{1−x}N$ ($0 \leq x \leq 1$) are studied using density functional theory. The change of lattice parameters with increased B composition shows small bowing parameters and thus slightly nonlinearity. The bandgap exhibits strong dependence on the B composition, where transition from direct to indirect bandgap occurs at a relatively low B composition ($x \sim 0.12$) is observed, above which the bandgap of $B_xAl_{1−x}N$ maintained indirect, thus desirable for low-absorption optical structures. The Γ_v-A_c and Γ_v-K_c indirect bandgaps are dominant at lower and higher B compositions, respectively. Density of states (DOS) of the valence band is susceptible to the B incorporation. Strong hybridization of Al, B, and N in p-states leads to high DOS near the valence band maximum. The hybridization of Al and B in s-states at lower B compositions and p-states of B at higher B compositions give rise to high DOS near lower end of the upper valence band. Charge density analysis reveals the B-N chemical bond is more covalent than the Al-N bond. This will lead to more covalent crystal with increasing B composition. Dramatic change of the heavy hole effective mass is found due to significant curvature increase of the band by minor B incorporation.

1 Introduction Conventional wurtzite (WZ) III-nitrides materials have attracted great attention owing to their excellent structural and electronic properties for device applications. Especially, $Al_xGa_{1−x}N$ alloys with tunable direct bandgap which can cover a wide ultraviolet (UV) spectral region (200–360 nm), have driven intense research in the development of UV devices recently [1].

WZ $B_xAl_{1−x}N$ alloys are expected to possess similar material properties such as high chemical stability and wide bandgap for UV device applications. Recently, a few groups have grown $B_xAl_{1−x}N$ epitaxially and measured its optical properties, which show effective refractive index modification by minor boron (B) incorporation [2, 3]. High reflectivity distributed Bragg reflectors (DBRs) have been demonstrated by employing high refractive index contrast $B_xAl_{1−x}N$/AlN structures [3]. Also, theoretical studies indicated the benefits of introducing B in the active region for optoelectronics, where UV light emission could be enhanced by four times using $B_xAl_yGa_{1−x−y}N$/AlN quantum wells (QWs) [4].

Though those studies show the potentials of $B_xAl_{1−x}N$ alloys, many issues have yet to be solved. For example, due to the phase separation, short diffusion length of B, and strong parasitic reaction in the gas phase, the B composition in the $B_xAl_{1−x}N$ alloys remains low [5]. Recently, a high B incorporation of 14.4% in a single-phase WZ BAlN was achieved with a thin layer of 100 nm [6]. Numerically, first-principle calculations of zinc-blende (ZB) $B_xAl_{1−x}N$ have been done [7, 8], where a small bowing parameter of lattice constants was observed and a first transition from indirect bandgap to direct bandgap occurred at a low B composition of 0.12. Furthermore, with an increased B composition, a second transition from direct back to indirect bandgap was found to happen at a higher B composition of 0.71.

While these results provided us with insights for understanding ZB $B_xAl_{1−x}N$, similar studies of WZ $B_xAl_{1−x}N$ have been absent. For the III-nitride device applications, however, the WZ structure is preferable and thermally stable [9]. Thus, the investigations of important

Phys. Status Solidi B 254, No. 8 (2017)

(2 of 8) 1600749

structural and electronic properties of WZ $B_xAl_{1-x}N$ alloys are urgently needed for further research and development.

In this work, the structural and electronic properties of $B_xAl_{1-x}N$ are systematically studied through first-principles calculation based on density functional theory (DFT). Details of the method are outlined in Section 2. In Section 3, the main results obtained from our calculations are presented and discussed. The conclusions are summarized in Section 4.

2 Computational method The DFT calculation was carried out by the MedeA-VASP simulation software [10]. For the exchange-correlation energy functional, we chose local density approximation (LDA). The ionic potentials were represented by the projector augmented wave (PAW) method. To cover different compositions of B, the supercell approach is applied. The structure size varies from 72-atoms ($3 \times 3 \times 2$) to primitive cell, which corresponds to the $B_xAl_{1-x}N$ alloys with different B compositions. The plane wave energy cut off was set in 400 eV and a higher cut off energy of 520 eV was applied in the primitive cells for the accuracy of relevant properties. In the optimization process, all the structures have been fully relaxed with the Hellman–Feynman force less than $0.02 \, \text{eV} \, \mathring{A}^{-1}$. The Monkhorst–Pack method is used with the grid being gamma-centered. Different Monkhorst–Pack k-point meshes were generated for different supercell sizes: $4 \times 4 \times 4$ for 72-atoms supercell, $6 \times 6 \times 4$ for 32-atoms supercell, and $6 \times 6 \times 6$ for 16-atoms supercell. For the density of states (DOS) and effective mass calculation, denser k-point meshes of $8 \times 8 \times 8$ and $13 \times 13 \times 13$ were applied.

It is well known that the standard exchange-correlations like the LDA or generalized gradient approximation (GGA) will underestimate of the energy bandgap in semiconductors [11]. Hybrid-functional DFT calculations with nonlocal exchange correlations like Heyd, Scueria, and Ernzerhof (HSE) are able to predict the bandgap in semiconductors more accurately [12]. However, they consume enormously computational resources than normal DFT calculation [13]. In addition, the HSE functional has been shown to underestimate the bandgap of WZ AlN considerably by 0.6–0.8 eV [14, 15], which can likely apply to BAlN alloys. In comparison, the scissors operation is a more efficient tool for the studied alloys [16]. By applying the scissor operator [17], the approximation formula of ternary alloys can be extracted following the Vegard's law [18–20]:

$$E_g(x) = (1-x)\left[E_{g,\text{AlN}}(\text{corrected}) - E_{g,\text{AlN}}(\text{LDA})\right]$$
$$+ x\left[E_{g,\text{BN}}(\text{corrected}) - E_{g,\text{BN}}(\text{LDA})\right]$$
$$+ E_{g,B_xAl_{1-x}N}(\text{LDA}). \quad (1)$$

As WZ AlN and BN are direct and indirect bandgap materials, respectively, $E_{g,\text{AlN}}(\text{corrected})$ of 6.2 eV [21] and $E_{g,\text{BN}}(\text{corrected})$ of 6.8 eV [22] corresponding to the direct and indirect bandgap were used for scissors operation which lifted the conduction bands upwards. Thus, the direct and
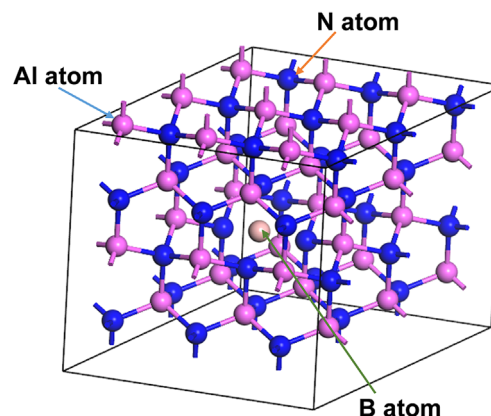

Figure 1 The $3 \times 3 \times 2$ BAlN supercell consists of 36 nitrogen (N) atoms, 35 aluminum (Al) atoms, and 1 boron (B) atom, corresponding to the 2.8% B composition.

indirect bandgap of $B_xAl_{1-x}N$ ($0 \leq x \leq 1$) can be obtained, such as the $\Gamma_v–K_c$ indirect bandgap of AlN and $\Gamma_v–\Gamma_c$ direct bandgap of BN (reported in Table 2).

The supercell approach is exemplarily shown in Fig. 1. The B-incorporated alloys are built mainly by substituting Al atoms by B atoms. In Fig. 1, the BAlN supercell consists of 72 atoms, including 36 N and 35 Al atoms, and 1 B atom. The substitution corresponds to the 2.8% B composition in this BAlN alloy. With increasing B composition, more B atoms will replace Al atoms. Considering the band folding effect and calculation time, we chose smaller supercell sizes such as 32 atoms supercell for B compositions of 6.25 and 87.5%, and 16 atoms supercell for B compositions of 12.5 and 25%, 50%, 75% for these compositions of interest.

3 Results and discussion
3.1 Structural properties Table 1 lists calculated lattice constants of some $B_xAl_{1-x}N$. It is noted that the

Table 1 The lattice constants for WZ AlN, BN, and $B_xAl_{1-x}N$.

material		a ($\mathring{A}$)	c ($\mathring{A}$)
AlN	this work	3.091	4.95
	exp.	3.11[a]	4.98[a]
	other cal.	3.13[b]	5.09[b]
	other cal.	3.112[c]	4.995[c]
	other cal.	3.124[d]	5.006[d]
$B_{0.028}Al_{0.972}N$	this work	3.062	4.896
$B_{0.25}Al_{0.75}N$	this work	2.98	4.693
$B_{0.5}Al_{0.5}N$	this work	2.87	4.465
$B_{0.75}Al_{0.25}N$	this work	2.694	4.344
BN	this work	2.525	4.179
	exp.	2.553[a]	4.215[a]
	exp.	2.558[e]	4.228[e]
	other cal.	2.500[f]	4.169[f]
	other cal.	2.534[d]	4.191[d]

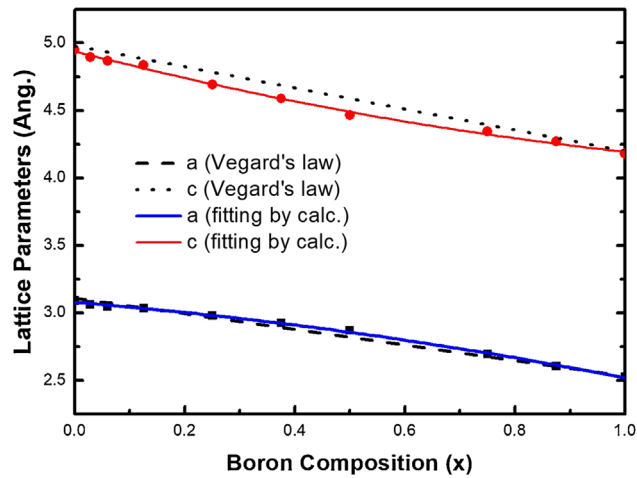[a]Ref. [23], [b]Ref. [24], [c]Ref. [25], [d]Ref. [27], [e]Ref. [26], [f]Ref. [18].

Figure 2 The calculated lattice constants of $B_xAl_{1-x}N$ alloy as a function of B composition.

lattice constants of binary compounds AlN and BN are in good agreement both with experimental and theoretical results. Furthermore, the lattice constants as a function of B composition, together with the linear interpolation from the Vegard's law are plotted in Fig. 2. The calculated results are fitted with polynomial Eqs. (2) and (3):

$$a\,(\overset{\circ}{A}) = 3.077 - 0.323x - 0.236x^2, \qquad (2)$$

$$c\,(\overset{\circ}{A}) = 4.940 - 1.052x + 0.307x^2. \qquad (3)$$

The bowing parameters $b_a = -0.236$ and $b_c = 0.307$ show slightly deviations from linearity for lattice constants a and c. This may result from the chemical bonding difference between AlN and BN. Besides, a relatively small supercell size could lead to the structural deviation [8].

3.2 Band structures The calculated band structures and DOS of WZ AlN and BN are shown in Fig. 3. AlN manifests a large direct bandgap of 6.2 eV in Fig. 3(a). Between Γ and K points there is an indirect bandgap of 6.7 eV. For BN, an indirect bandgap is observed and the gap between Γ and K points is 6.8 eV, as shown in Fig. 3 (b). BN also shows a direct bandgap of 10.2 eV. The bandgap of AlN and BN from this study and previous reports are summarized in Table 2, which show good agreement.

The band structures of $B_xAl_{1-x}N$ with varying B compositions are shown in Fig. 4(a)–(h). All the energies are with reference to the top of the valence band. Furthermore, the direct and indirect bandgap energies are extracted and plotted in Fig. 5. At the B composition equals to zero, i.e., AlN, the direct bandgap is smaller than the indirect bandgap. With increased B compositions, both direct and indirect bandgaps reduce, where the indirect bandgap decreases faster. A direct–indirect bandgap transition is observed, happening at a relatively low B composition around 0.125. Above this composition, both
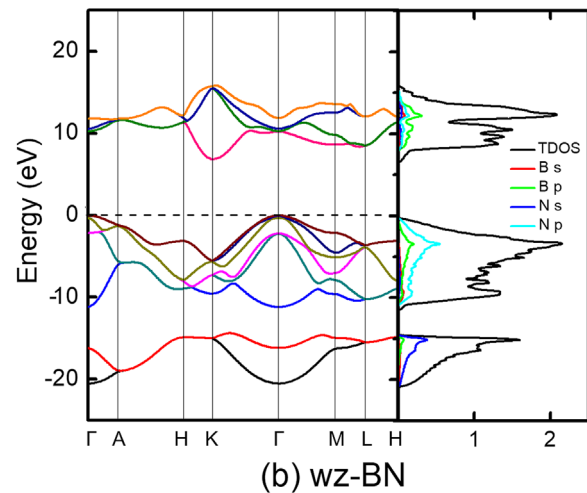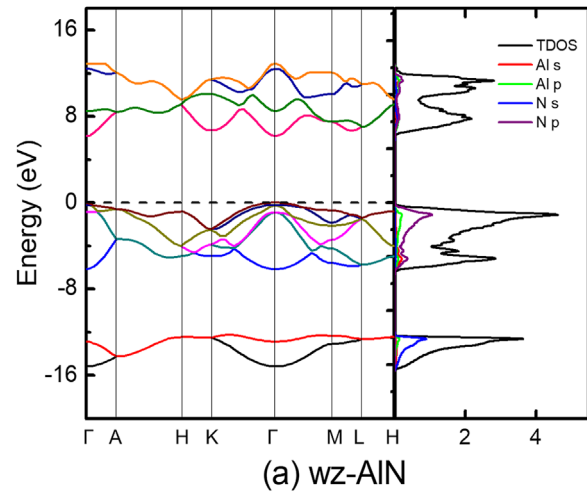

Figure 3 Band structures with partial DOS (PDOS) and total DOS (TDOS) of WZ (a) AlN and (b) BN.

direct and indirect bandgaps continue to decrease until at $x = \sim 0.3$. Above that, both bandgaps increase as a function of B composition. However, the bandgap transition is not observed and thus the indirect bandgap prevails

Table 2 The calculated and corrected bandgap (eV) of WZ AlN and BN.

	bandgap (unit: eV)			
compound	this work	corrected calc.	other calc.	experimental
AlN				
Γ_v–Γ_c	4.4	6.2	4.26[a] (LDA)	6.02[b]
Γ_v–K_c	4.9	6.7	5.16[a] (LDA)	–
BN				
Γ_v–Γ_c	8.3	10.2	4.5[c] (LDA)	–
Γ_v–K_c	4.9	6.8	6.86[d] (GW)	–
			10.43[d] (GW)	

[a]Ref. [27], [b]Ref. [21], [c]Ref. [18], [d]Ref. [22].

Original

Paper

Phys. Status Solidi B 254, No. 8 (2017)
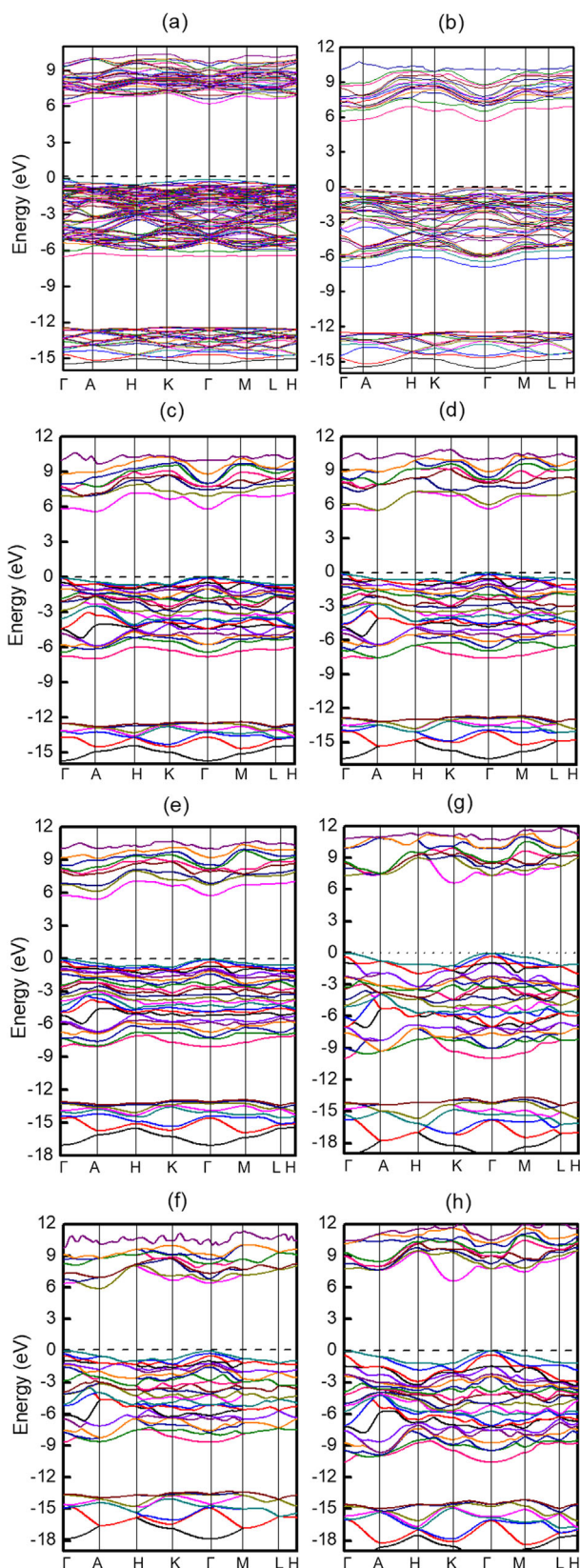
(4 of 8) 1600749

(a) (b) (c) (d) (e) (g) (f) (h)

Figure 4 Band structures of $B_xAl_{1-x}N$ with different B compositions. From (a) to (h), x equals to 2.8, 6.25, 12.5, 25, 37.5, 50, 75, 87.5%.
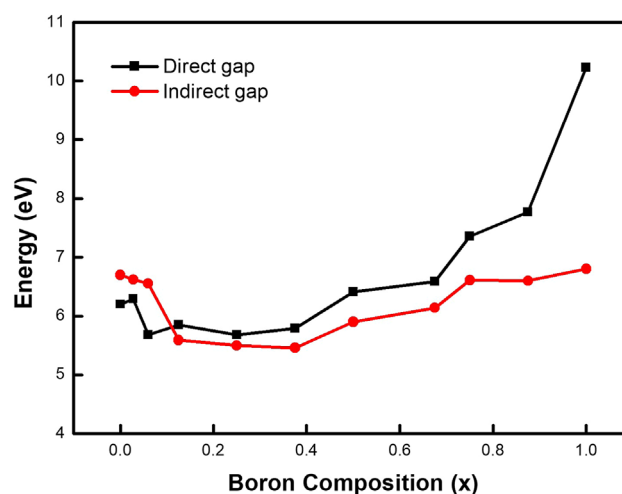

Figure 5 The bandgap energy of $B_xAl_{1-x}N$ as a function of B composition.

above the B composition of 0.125. This hints that $B_xAl_{1-x}N$ ($x > 0.125$) can be weakly absorptive and be potentially utilized for structures that require high UV transparency such as DBRs. In comparison, there are two, i.e., indirect–direct and direct–indirect, transitions at $x = 0.12$ and 0.71 with an increased B composition, respectively, for ZB $B_xAl_{1-x}N$ [7, 8]. It is also noted that the direct bandgap increases much faster than the indirect bandgap at B compositions higher than 0.7.

The variation of direct and indirect bandgap energies as a function of the B composition is further broken down in Fig. 6. It is noted that the Γ_v–K_c indirect bandgap is stable around 6.5–7.0 eV and is the dominant indirect bandgap at smaller ($< \sim 0.05$) and larger ($> \sim 0.7$) B compositions. On the contrary, large variation of the Γ_v–A_c indirect bandgap occurs at the smaller and larger B compositions. At
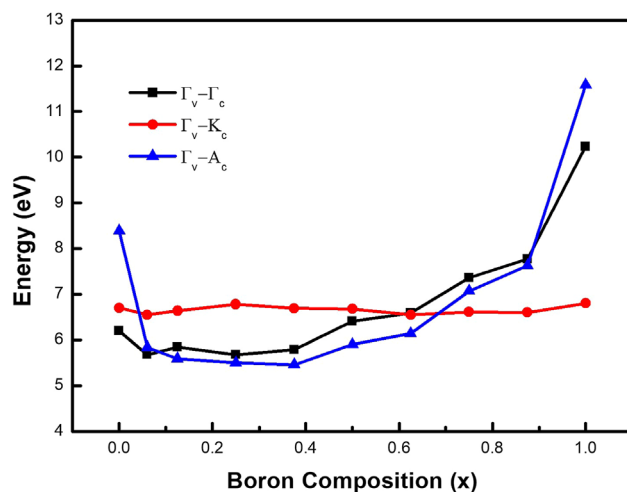

Figure 6 The comparison of the energy bandgap of $B_xAl_{1-x}N$ as a function of B composition at different high symmetry points.
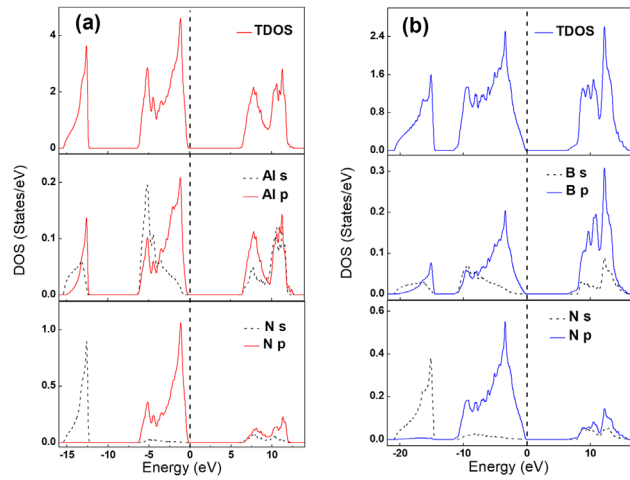
Figure 7 The TDOS and PDOS the $6 \times 6 \times 6$ k-grid of (a) AlN and (b) BN.

$\sim 0.05 < x < 0.7$, the Γ_v–A_c indirect bandgap remains relatively stable and is the dominant indirect bandgap. In comparison, the Γ_v–X_c bandgap is always the dominant indirect bandgap for ZB $B_xAl_{1-x}N$ [7, 8].

3.3 Density of states (DOS) The PDOS and TDOS of the $B_xAl_{1-x}N$ alloys were shown in Figs. 7 and 8. We adopted a denser k-grid of $8 \times 8 \times 8$ for $B_{0.25}Al_{0.75}N$, $B_{0.5}Al_{0.5}N$ and $B_{0.75}Al_{0.25}N$, to ensure the accuracy of the DOS. Three regions of DOS are distinct, i.e., the upper and the lower valence bands, and the conduction bands. For AlN, the upper valence bands are dominated by the p-states

of N, while the s-states of N occupies the lower valence bands, as shown in Fig. 7(a). All the orbitals contribute to the conduction band, rather than by certain states. For BN, however, the conduction band of BN is mainly contributed by the p-states of B, as shown in Fig. 7(b). The calculated DOS of AlN and BN shows good agreement with previous results [27, 28].

In the PDOS calculation for different B compositions of BAlN, the peak at the lower valence band ($\sim$$-15$ eV) is always dominated by N s-states, as shown in Fig. 8. As a result, the charge could transfer from Al (or B) to N due to the electronegativity difference between N and Al (or B) [7]. In the upper valence band, two significant peaks exist in the TDOS of $B_xAl_{1-x}N$ ($0 < x < 1$, except $x = 0.5$) as highlighted by the arrows, albeit the peak position and formation have slightly difference. Due to strong hybridization of Al, B, and N in p-states, the peak which has higher energy near the valence band maximum (VBM) shows high DOS and it is the highest peak in $B_xAl_{1-x}N$ ($0 < x < 1$), indicating the highly localized charges at this energy level. For the second significant peak with lower energy as shown in Fig. 8(a), the peak is dominated by the hybrid s-states of Al and B when the B composition is low, such as $B_{0.25}Al_{0.75}N$. When x equals to 0.5, the p-states peak of B shifts to a deeper energy, so second peak is submerged because of the hybridization of the s-states and p-states of B. After introducing more B (seen as $B_{0.75}Al_{0.25}N$), p-states of B becomes stronger than s-states of B, so the second peak arises again and gets closer to the VBM. Unlike the second peaks in alloys with low B compositions, this peak is mainly attributed to the p-states peak of B.
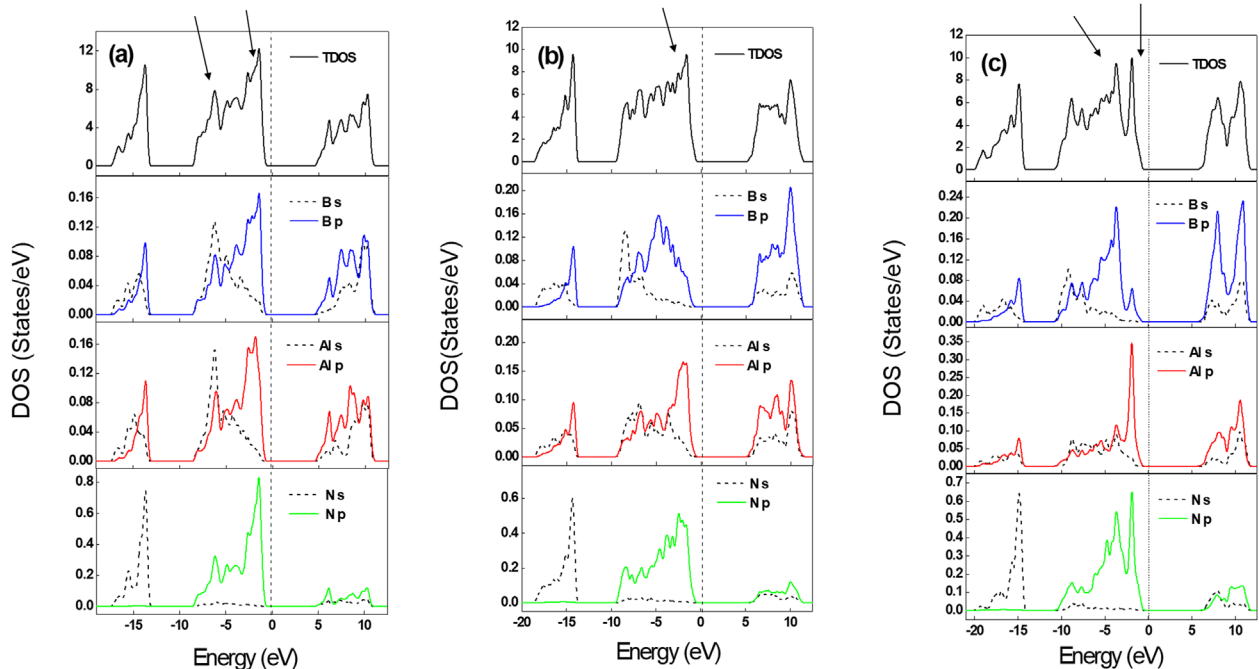

Figure 8 The TDOS and PDOS with the $8 \times 8 \times 8$ k-grid of (a) $B_{0.25}Al_{0.75}N$, (b) $B_{0.5}Al_{0.5}N$, and (c) $B_{0.75}Al_{0.25}N$. The black arrows refer to the significant peaks in the upper valence bands.
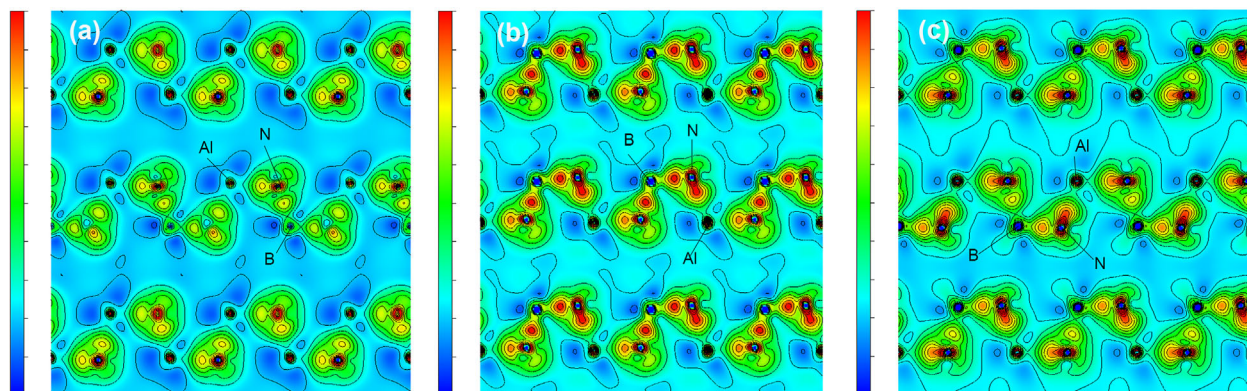
Original

Paper

Phys. Status Solidi B 254, No. 8 (2017)

(6 of 8) 1600749

Figure 9 The 2D deformation charge density maps of (1 1 0) planes of (a) $B_{0.25}Al_{0.75}N$, (b) $B_{0.5}Al_{0.5}N$, and (c) $B_{0.75}Al_{0.25}N$.

3.4 Charge density analysis Besides the DOS, we can further investigate the electronic properties by deformation charge density, which is an intuitionistic tool to observe charge transfer in the crystal. As shown in Fig. 9, positive (warmer color) area in the map mostly arranges around N atoms, which area means the charges will assemble. Furthermore, it is clearly confirmed that the charges are more likely to be transferred from Al atoms to N atoms than from B atoms to N atoms. In other words, the Al–N bonds are ironic and the B–N bonds are more covalent, which is consistent with electronegativity of those elements. Meanwhile, the crystals are likely to become more covalent with the B composition increased, due to the B–N and Al–N chemical bonds characteristics.

The chemical bond properties can be further confirmed by the Bader analysis. In Table 3, the charge transfer situation of each atom from the Bader charge analysis of BAlN are summarized. For example, in $B_{0.5}Al_{0.5}N$, the amount of charge transfer from Al to N are more than from B to N due to the electronegativity as discussed above. The charge transfer situations at atom level in $B_{0.25}Al_{0.75}N$ and $B_{0.75}Al_{0.25}N$ are very similar to $B_{0.5}Al_{0.5}N$.

3.5 Effective mass The effective masses of the electron (m_e), heavy hole (m_{hh}), light hole (m_{lh}), and split-off hole (m_{sh}) of $B_xAl_{1-x}N$ are calculated from the band structures and listed in Table 4. Since the effective masses will not be the same at different directions in the k-space, we calculated the effective masses in k_z direction (parallel) and in k_xk_y direction (vertical), using the parabolic line fitting method. The adjusted R-squared number of all our fittings are above 0.99, which means the parabolic fitting of the bands is reasonable and suitable. The calculated effective masses of AlN match well with previous results [30, 31], as listed in Table 4. The average effective mass of $B_xAl_{1-x}N$ is plotted in Fig. 10. The effective mass of heavy holes decreases with minor B incorporation dramatically, indicating much increased curvature for the heavy hole band. Meanwhile, the variation of effective masses of light holes and split-off holes is much less significant. This phenomenon indicates a drastic change happening in the valence band. On one hand, unlike the light and split-off holes, the effective mass of heavy hole of AlN is much larger than BN. On the other hand, it has been reported that the localized energy band could be formed near the uppermost valence band by incorporating phosphorus atoms into GaN [29]. Similarly, when B atoms introduced into the AlN, the corresponding energy band near the uppermost valence band can significantly be re-shaped due to considerably changed effective mass.

Table 3 The Bader analysis results of $B_{0.25}Al_{0.75}N$, $B_{0.5}Al_{0.5}N$, and $B_{0.75}Al_{0.25}N$.

alloy	atoms	valence charge	charge transfer	volume ($\mathring{A}^3$)	distance ($\mathring{A}$)
$B_{0.25}Al_{0.75}N$	B	0.9279	2.0721	2.1965	0.4181
	N1	7.1927	−2.1927	13.8079	0.9929
	Al	0.6825	2.3175	4.0542	0.00406
	N2	7.2524	−2.2524	14.6329	0.9896
$B_{0.5}Al_{0.5}N$	B	0.9490	2.0510	2.1851	0.3915
	N1	7.0882	−2.0882	12.3173	0.9704
	Al	0.6828	2.3172	3.8310	0.0347
	N2	7.2800	−2.2800	12.9978	0.9006
$B_{0.75}Al_{0.25}N$	B	0.9478	2.0522	2.0369	0.4404
	N1	7.1448	−2.1448	10.9838	0.9204
	Al	0.6666	2.3334	3.6196	0.0274
	N2	7.0698	−2.0698	12.0132	1.0084

Table 4 The calculated effective masses of WZ $B_xAl_{1-x}N$ ($x = 0$, 0.25, 0.5, 0.75, 1).

| unit: m_0	AlN	$B_{0.06}Al_{0.94}N$	$B_{0.25}Al_{0.75}N$	$B_{0.5}Al_{0.5}N$	$B_{0.75}Al_{0.25}N$	BN	AlN ref.	BN ref.
$m_e^\perp$	0.32	0.32	0.44	0.31	0.58	0.52	0.31[a], 0.35[b]	0.35[c]
$m_e^\|$	0.32	0.29	0.28	0.48	0.31	0.33	0.32[a], 0.35[b]	0.24[c]
$m_{hh}^\perp$	10.04	2.72	0.37	1.57	1.38	1.82	11.11[a], 1.14[b]	1.02[c]
$m_{hh}^\|$	2.97	0.77	3.27	1.77	3.63	1.37	2.94[a], 3.53[b]	1.08[c]
$m_{lh}^\perp$	0.32	0.40	1.35	0.52	0.46	0.40	0.26[a], 0.33[b]	–
$m_{lh}^\|$	2.97	0.77	0.28	0.33	2.03	1.37	2.94[a], 3.53[b]	–
$m_{sh}^\perp$	2.51	1.57	1.35	0.35	0.80	1.82	3.57[a], 4.05[b]	–
$m_{sh}^\|$	0.26	0.29	0.28	2.07	0.31	0.27	0.25[a], 0.26[b]	–

[a]Ref. [30], [b]Ref. [31], [c]Ref. [32].
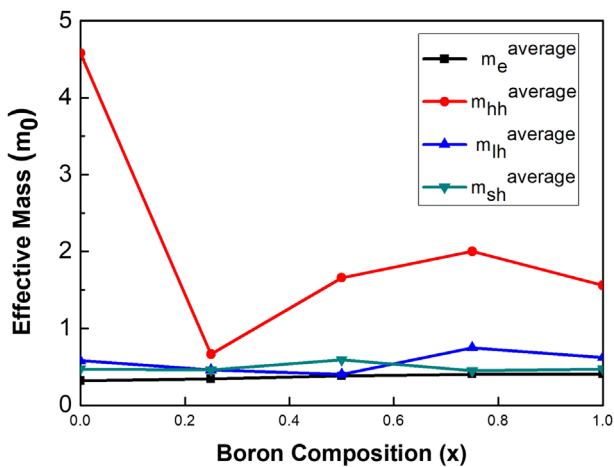
Figure 10 The average effective masses of electrons, heavy holes, light holes, and split-off holes of BAlN obtained from Table 4.

4 Conclusions In summary, the structural and electronic properties of WZ $B_xAl_{1-x}N$ are investigated by first-principles calculations. The calculation of AlN and BN shows good agreements with previous theoretical and experimental works. For $B_xAl_{1-x}N$, the change of lattice parameters exhibits slight nonlinearity with respect to the B compositions. A transition from direct to indirect bandgap happens at a relatively low B composition (~12%). The Γ_v–A_c and Γ_v–K_c indirect bandgaps are found to be dominant at lower and higher B compositions, respectively. This property is desirable for low-absorption optical structures. We use the DOS to analyze the charges distribution and find that the upper valence band is modified mostly with varying B compositions. Furthermore, the charge density analysis infers that the crystal will be more covalent with increasing B composition. Finally, dramatically variation of heavy holes is observed due to the B incorporation.

References

[1] T. D. Moustakas, MRS Commun. **6**, 247 (2016).

[2] S. Watanabe, T. Takano, K. Jinen, J. Yamamoto, and H. Ka-wanishi, Phys. Status Solidi C **7**, 2691 (2003).

[3] M. Abid, T. Moudakir, G. Orsal, S. Gautier, A. En. Naciri, Z. Djebbour, J. H. Ryou, G. Patriarche, L. Largeau, H. J. Kim, Z. Lochner, K. Pantzas, D. Alamarguy, F. Jomard, R. D. Dupuis, J. P. Salvestrini, P. L. Voss, and A. Ougazzaden, Appl. Phys. Lett. **100**, 051101 (2012).

[4] S. H. Park and D. Ahn, Appl. Phys. Express **9**, 02100 (2016).

[5] X. Li, S. Sundaram, Y. El Gmili, F. Genty, S. Bouchoule, G. Patriache, P. Disseix, F. Re veret, J. Leymarie, J. P. Salvestrini, R. D. Dupuis, P. L. Voss, and A. Ougazzaden, J. Cryst. Growth **414**, 119 (2015).

[6] X. Li, S. Wang, H. Liu, F. A. Ponce, T. Detchprohm, and R. D. Dupuis, Phys. Status Solidi B (2017). https://doi.org/10.1002/pssb.201600699

[7] R. Riane, R. Boussahl, Z. Zaoui, A. Hammerelaine, and L. Matar, Solid State Sci. **11**, 200 (2009).

[8] S. Kumar, S. Joshi, B. Joshi, and S. Auluck, J. Phys. Chem. Solids **86**, 101 (2015).

[9] P. Lawaetz, Phys. Rev. B **4**, 3460 (1971).

[10] MedeA® 2.20.1, Materials Design, Inc., Angel Fire, NM 87710, USA (2016).

[11] R. O. Jones and O. Gunnarsson, Rev. Mod. Phys. **61**, 689 (1989).

[12] H. Xiao, J. Tahir-Kheli, J. Goddard, and W. A. Goddard III, J. Phys. Chem. Lett. **2**, 212 (2011).

[13] J. M. Crowley, J. Tahir-Kheli, and W. A. Goddard III, Jpn. J. Appl. Phys. **7**, 1198 (2016).

[14] I. H. Nwigboji, J. I. Ejembi., Y. Malozovsky, B. Khamala, L. Franklin, G. Zhao, C. E. Ekuma, and D. Bagayoko, Mater. Chem. Phys. **157**, 86 (2015).

[15] Our calculation shows WZ AlN's direct bandgap is 5.4 eV by using the HSE06 functional, which is about 0.8 eV smaller than the experimentally determined value.

[16] Z. H. Levine and D. C. Allan, Phys. Rev. Lett. **63**, 1719 (1989).

[17] Z. H. Levine and D. C. Allan, Phys. Rev. B **43**(5), 4187 (1991).

[18] A. Said, M. Debbichi, and M. Said, Optik **127**, 9212 (2016).

[19] I. Vurgaftman, J. R. Meyer, and L. R. Ram-Mohan, J. Appl. Phys. **89**, 5815 (2001).

[20] I. Gorczyca, S. P. Lepkowski, T. Suski, N. E. Christensen, and A. Svane, Phys. Rev. B **80**, 075202 (2009).

Phys. Status Solidi B 254, No. 8 (2017)

Original
Paper

(8 of 8) 1600749

[21] H. Yamashita, K. Fukui, S. Misawa, and S. Yoshida, J. Appl. Phys. **50**, 896 (1979).

[22] S. P. Gao, Comput. Mater. Sci. **61**, 266 (2012).

[23] J. H. Edgar (ed.), Properties of Group III Nitrides, EMIS Datareviews Series No. 11 (INSPEC, The Institution of Electrical Engineers, London, 1994).

[24] V. I. Gavrilenko and R. Q. Wu, Phys. Rev. B **61**, 2632 (2000).

[25] K. Shimada, T. Sota, and K. Suzuki, J. Appl. Phys. **84**, 4951 (1998).

[26] T. Soma, A. Sawaoka, and S. Saito, Mater. Res. Bull. **7**, 755 (1974).

[27] Z. Jiao, S. Ma, and J. Yang, Solid State Sci. **13**, 33 (2011).

[28] R. F. Zhang, S. Veprek, and A. S. Argon, Phys. Rev. B **77**, 172103 (2008).

[29] C. K. Tan, D. Borovac, W. Sun, and N. Tansu, Sci. Rep. **6**, 24412 (2016).

[30] A. Punya and W. R. L. Lambrecht, Phys. Rev. B **85**, 195147 (2012).

[31] K. Kim, W. L. R. Lambrecht, B. Segall, and M. van Schilfgaarde, Phys. Rev. B **56**, 7363 (1997).

[32] Y. N. Xu and W. Y. Ching, Phys. Rev. B **44**, 7787 (1991).